Inorganic Chemistry

Article

pubs.acs.org/IC

Synthesis, Characterization, and Materials Chemistry of Group 4 Silylimides

S. D. Cosham,[†] A. L. Johnson,*[,†] K. C. Molloy,[†] and Andrew J. Kingsley[‡]

[†]Department of Chemistry, University of Bath, Claverton Down, Bath BA2 7AY, United Kingdom

[‡]SAFC-Hitech, Power Road, Bromborough, Wirral, CH62 3QF, United Kingdom

Supporting Information

ABSTRACT: This paper focuses on the development of potential single source precursors for M−N−Si (M = Ti, Zr or Hf) thin films. The titanium, zirconium, and hafnium silylimides $(Me_2N)_2MNSiR^1R^2R^3$ [$R^1 = R^2 = R^3$ = Ph, M = Ti(**1**), Zr (**2**), Hf (**3**); $R^1 = R^2 = R^3$ = Et, M = Ti (**4**), Zr (**5**), Hf (**6**); $R^1 = R^2$ = Me, $R^3 = {}^t$Bu, M = Ti (**7**), Zr (**8**), Hf (**9**); $R^1 = R^2 = R^3 = NMe_2$, M = Ti (**10**), Zr (**11**), Hf (**12**)] have been synthesized by the reaction of $M(NMe_2)_4$ and $R^3R^2R^1SiNH_2$. All compounds are notably sensitive to air and moisture. Compounds **1**, **2**, **4**, and **7**−**10** have been structurally characterized, and all are dimeric, with the general formula $[M(NMe_2)_2(\mu\text{-}NSiR_3)]_2$, in which the μ_2-$NSiR_3$ groups bridges two four-coordinate metal centers. The hafnium compound **3** possesses the same basic dimeric structure but shows additional incorporation of liberated $HNMe_2$ bonded to one metal. Compounds **11** and **12** are also both dimeric but also incorporate additional μ_2-NMe_2 groups, which bridge Si and either Zr or Hf metal centers in the solid state. The Zr and Hf metal centers are both five-coordinated in these species. Aerosol-assisted CVD (AA-CVD) using **4**−**7** and **9**−**12** as precursors generates amorphous films containing M, N, Si, C, and O; the films are dominated by MO_2 with smaller contributions from MN, MC and MSiON based on XPS binding energies.

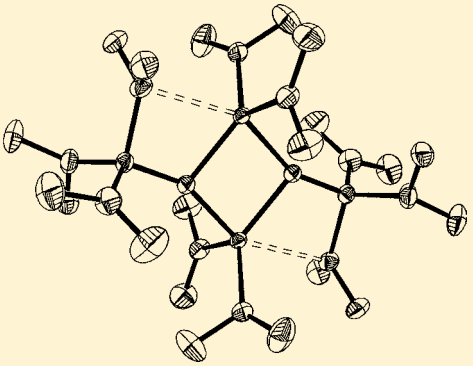

INTRODUCTION

The production of metallic thin films by chemical vapor deposition (CVD) or, more recently, atomic layer deposition (ALD) has been an area of significant interest to those in the microelectronics industry for the past three decades, mainly due to numerous potential applications in which these materials can be exploited. During this time, the deposition of metal nitrides has continually been at the forefront of research and continually cited in the International Roadmap for Semiconductors as an area of considerable interest.[1] As the size downscaling of microelectronics continues, and the use of copper as an interconnect material in integrated circuitry has increased,[2] the need for materials that can inhibit the fast diffusion of copper into the underlying silicon layers, and prohibit the formation of highly resistive materials such as Cu_3Si, has increased.[3]

Refractory nitrides of the early transition metals (Groups 4−6) have become increasingly important as diffusion barrier layers in ultra-large-scale integrated devices (ULSI), and while historically Ti−N has been the barrier most widely studied,[4] Hf−N, Zr−N, Ta−N, and Nb−N[5] have also attracted interest due to a favorable combination of high conductivity, thermal stability, and chemical inertness. However, one of the drawbacks of crystalline barrier materials, such as Ti−N, is the diffusion of Cu along grain boundaries.[6] As a result, there is increasing attraction toward amorphous ternary materials such as M−Si−N (M = Ti, Ta, W, Mo) and, to a lesser extent, M−B−N.[7] The efficacy of these films is sensitive to the relative M/N/Si ratios, with a high N content raising the temperature at which crystallization commences,[8] while excessive Si broadly encourages the formation of regions of resistive Si_3N_4 within the films.[7,9]

To date, the deposition of these ternary films has been largely by physical vapor deposition techniques such as cathodic arc ion plating (Ti−Si−N),[6d,10] sputtering in a nitrogen atmosphere (Ti−Si−N,[11] Ta−Si−N,[8,12] W−Si−N[12,13]) or co-sputtering (Hf−Si−N,[14] Nb−Si−N,[15] Ta−Si−N,[12,14] Mo−Si−N[12,14]), and ion-beam assisted deposition (Ti−B−N).[16] Variations on chemical vapor deposition (CVD) methods have all been from multiple sources, e.g., MOCVD (Ti−Si−N[9,14,17]), LPCVD (Ti−Si−N,[18] Ta−Si−N,[18b] W−Si−N,[18b] Re−Si−N[18b]), PECVD (Ta−C−N[19]), and ALD (Ti−Si−N,[20] and various others[21]). To our knowledge, there is only one example in the literature where a single-source precursor, namely, $[(NMe_2)_3Si\{H\}N)_2Ti(\mu_2\text{-}NSi(NMe_2)_3)]_2$, has been used to deposit mesoporous M−Si−N material under high temperature ammonolysis conditions. However, several examples are found in the patent literature, which claim the use of metal complexes of bidentate silylamides, i.e. $[R_2Si(NR')_2]_xMNR''_2$, for the formation of M−Si−N thin film materials using CVD methods for a range of metals from Groups 4−6;[22] details of the characterization of these complexes were, however, not included in these patents. It is important to note that a successful single-source precursor capable of depositing carbon

Received: July 21, 2011
Published: November 4, 2011

and oxygen-free early transition metal MN or M−Si−N films has yet to be reported in a non-patent report. Typically, precursors also require an external/additional reactive source of nitrogen (e.g., ammonia or hydrazine) to produce MN or M−Si−N thin films. It is for these reasons that the development of new single-source precursors represents a significant challenge.

Our interest in this area is the synthesis and development of single source precursors that contain preformed M−N−Si linkages for CVD purposes.[23] While there is a paucity of complexes developed specifically for utilization in CVD applications, it is important to note that there are a wide range of complexes reported in the literature that have been developed for catalytic purposes which contain both preformed M−N−Si linkages and an $\{MN_4\}$ core which is expected to favor formation of M−N materials on decomposition.[24]

In this paper, we report on the reactions of $M(NMe_2)_4$ (M = Ti, Zr, Hf) with a variety of silylamines, the structural and spectroscopic characterization of the products, and an assessment of the utility of selected species to form amorphous M−Si−N films by aerosol-assisted CVD (AACVD).

EXPERIMENTAL SECTION

All operations were carried out under an atmosphere of dry dinitrogen or argon using standard Schlenk and glovebox techniques. Hexane, toluene, pentane, dichloromethane, and diethyl ether solvents were dried using an Innovative Technology, Inc. Solvent Purification System (SPS) system and degassed under dinitrogen or argon prior to use. Deuterated benzene (C_6D_6) NMR solvent was purchased from Aldrich and dried by refluxing over potassium before isolating by vacuum distillation. All dry solvents were stored under dinitrogen or argon in Young's flasks over 4 Å molecular sieves.

Tetrakis(dimethylamino)metal derivatives (Ti, Zr, Hf) were used as supplied by SAFC HiTech. The silylamine compounds $[Ph_3SiNH_2]$,[25] $[Et_3SiNH_2]$,[25] $[^tBuMe_2SiNH_2]$,[26] and $[(Me_2N)_3SiNH_2]$[27] were prepared by literature procedures.

Solution ^1H and ^{13}C NMR experiments were performed at ambient temperature using a Bruker Avance-300, and ^{29}Si NMR experiments were performed at ambient temperature using a Bruker Advance-500. ^1H and ^{13}C NMR chemical shifts are referenced internally to residual nondeuterated solvent resonances. All chemical shifts are reported in δ (ppm) and coupling constants in Hz. Elemental analyses were performed externally by London Metropolitan University Elemental Analysis Service.

Thermogravimetric analyses (TGA) were performed at SAFC Hitech using a Shimadzu TGA-51 Thermogravimetric Analyzer, while SEM analysis of the films was undertaken on a JEOL JSM-6480LV scanning electron microscope with EDX capability. X-ray photoelectron spectroscopy analyses were performed on a Kratos Axis Ultra-DLD XPS system at the Wolfson Nanoscience Laboratory Service at Cardiff University. The elemental compositions of the films deposited using **4**−**10** and **12** as the precursors have been quantitatively determined by XPS, with sputter etching of the films to achieve a qualitative depth profile. The film was sputter-etched over a 2 mm^2 area, with the center of this area analyzed using a 100 μm spot.

Synthesis of $[\{(Me_2N)_2Ti(\mu_2\text{-}NSiPh_3)\}_2]$ (1). A stirred toluene (20 mL) solution of Ph_3SiNH_2 (1.11 g, 4.0 mmol) was treated with a toluene solution (30 mL) of $Ti(NMe_2)_4$ (0.90 g, 4.0 mmol). Solution was heated to 70 °C for 24 h, and the volume then halved under reduced pressure. Crystallization from the reaction solution at −28 °C afforded $[\{(Me_2N)_2Ti(\mu_2\text{-}NSiPh_3)\}_2]$ (**1**) as orange crystals. Yield: 0.69 g, 45%. Analysis, found (calcd for $C_{44}H_{54}N_6Si_2Ti_2$): C, 64.7 (64.5); H, 6.5 (6.7); N, 10.4 (10.3)%. ^1H NMR (300 MHz, C_6D_6): δ_H 7.72−7.63 (br m, 6H, *ortho*-C_6H_5), 7.17−7.03 (br m, 9H, *meta*- and *para*-C_6H_5), 2.92 (s, 12H, NMe_2). $^{13}C\{^1H\}$ NMR (75.5 MHz, C_6D_6): δ_C 139.2 (*ipso*-C_6H_5), 136.0 (*ortho*-C_6H_5), 129.2 (*para*-C_6H_5), 45.0 (NMe_2). ^{29}Si NMR (99.35 MHz, C_6D_6): δ_{Si} −28.7.

Synthesis of $[\{(Me_2N)_2Zr(\mu_2\text{-}NSiPh_3)\}_2]$ (2). A stirred toluene (30 mL) solution of Ph_3SiNH_2 (2.75 g, 10.0 mmol) was treated with a toluene (20 mL) solution of $Zr(NMe_2)_4$ (2.67 g, 10.0 mmol). The solution was heated to 70 °C for 24 h, and the volume was then reduced under reduced pressure. Crystallization from the reaction solution at −28 °C affords $[\{(Me_2N)_2Zr(\mu_2\text{-}NSiPh_3)\}_2]$ (**2**) as white crystals. Yield: 2.48 g, 55%. Analysis, found (calcd for $C_{44}H_{54}N_6Si_2Zr_2$): C, 58.5 (58.4); H, 6.2 (6.0); N, 9.1 (9.3)%. ^1H NMR (300 MHz, C_6D_6): δ_H 7.87−7.83 (m, 6H, *ortho*-C_6H_5), 7.27−7.17 (br m, 9H, *meta*- and *para*-C_6H_5), 2.72 (s, 12H, NMe_2). $^{13}C\{^1H\}$ NMR (75.5 MHz, C_6D_6): δ_C 140.2 (*ipso*-C_6H_5), 135.9 (*ortho*-C_6H_5), 129.2 (*para*-C_6H_5), 127.9 (*meta*-C_6H_5), 42.2 (NMe_2). ^{29}Si NMR (99.35 MHz, C_6D_6): δ_{Si} −33.1.

Synthesis of $[\{(Me_2N)_2Hf(\mu_2\text{-}NSiPh_3)\}_2(HNMe_2)]$ (3). A stirred toluene (30 mL) solution of Ph_3SiNH_2 (2.75 g, 10.0 mmol) was treated with a toluene (20 mL) solution of $Hf(NMe_2)_4$ (3.56 g, 10.0 mmol). The solution was heated to 70 °C for 24 h and the volume then reduced under reduced pressure. Crystallization from the reaction solution at −28 °C afforded $[\{(Me_2N)_2Hf(\mu_2\text{-}NSiPh_3)\}_2(HNMe_2)]$ (**3**) as white crystals. Yield: 3.20 g, 57%. Analysis, found (calcd for $C_{46}H_{61}Hf_2N_7Si_2$): C, 48.9 (49.1); H, 5.4 (5.5); N, 8.6 (8.7)%. ^1H NMR (300 MHz, C_6D_6): δ_H 8.01−7.96 (m, 12H, *ortho*-C_6H_5), 7.39−7.25 (br m, 18H, *meta*- and *para*-C_6H_5), 2.86 (s, 24H, $HfNMe_2$), 1.60 (s, 6H, $HNMe_2$). $^{13}C\{^1H\}$ NMR (75.5 MHz, C_6D_6): δ_C 141.2 (*ipso*-C_6H_5), 136.6 (*ortho*-C_6H_5), 129.4 (*para*-C_6H_5), 127.2 (*meta*-C_6H_5),42.6 (Hf-NMe_2), 39.8 (Hf−N(H)Me_2). ^{29}Si NMR (99.35 MHz, C_6D_6): δ_{Si} −31.8.

Synthesis of $[\{(Me_2N)_2Ti(\mu_2\text{-}NSiEt_3)\}_2]$ (4). A stirred hexane (20 mL) solution of Et_3SiNH_2 (9.96 g, 76.0 mmol) was treated with a hexane (30 mL) solution of $Ti(NMe_2)_4$ (17.04 g, 76.0 mmol). After stirring for 24 h, volatiles were removed *in vacuo*. Recrystallization of the residue from hexane at −28 °C yielded $[\{(Me_2N)_2Ti(\mu_2\text{-}NSiEt_3)\}_2]$ (**4**) as orange crystals. Yield: 10.92 g, 54%. Analysis, found (calcd for $C_{20}H_{54}N_6Si_2Ti_2$): C, 45.3 (45.3); H, 9.9 (10.3); N, 15.6 (15.8)%. ^1H NMR (300 MHz, C_6D_6): δ_H 3.30 (s, 4H, NMe_2), 1.07 (t, 3H, CH_2CH_3, $^3J_{CH2\text{-}CH3}$ 7.8), 0.57 (q, 2H, CH_2CH_3, $^3J_{CH2\text{-}CH3}$ 7.8). $^{13}C\{^1H\}$ NMR (75.5 MHz, C_6D_6): δ_C 45.6 (s, 4C, NMe_2), 8.27 (s, 3C, CH_2CH_3), 7.45 (s, 3C, CH_2CH_3,). ^{29}Si NMR (99.35 MHz, C_6D_6): δ_{Si} −0.71.

Synthesis of $[\{(Me_2N)_2Zr(\mu_2\text{-}NSiEt_3)\}_2]$ (5). A stirred toluene (20 mL) solution of Et_3SiNH_2 (0.66 g, 5.0 mmol) was treated with a toluene (30 mL) solution of $Zr(NMe_2)_4$ (1.34 g, 5.0 mmol). After stirring for 24 h, volatiles were removed *in vacuo*. Recrystallization of the residue from hexane at −28 °C afforded $[\{(Me_2N)_2Zr(\mu_2\text{-}NSiEt_3)\}_2]$ (**5**) as pale yellow crystals. Due to the high solubility of **5** within hexane at room temperature, crystals were isolated at −20 °C using a NaCl ice bath. Yield: 0.33 g, 21%. Analysis, found (calcd for $C_{20}H_{54}N_6Si_2Zr_2$): C, 39.2 (38.9); H, 8.9 (8.8); N, 13.6 (13.6)%. ^1H NMR (300 MHz, C_6D_6): δ_H 3.10 (s, 4H, NMe_2), 1.10 (t, 3H, CH_2CH_3, $^3J_{CH2\text{-}CH3}$ 7.8), 0.58 (q, 2H, CH_2CH_3, $^3J_{CH2\text{-}CH3}$ 7.8). $^{13}C\{^1H\}$ NMR (75.5 MHz, C_6D_6): δ_C 42.5 (NMe_2), 8.61 (CH_2CH_3), 7.68 (CH_2CH_3,). ^{29}Si NMR (99.35 MHz, C_6D_6): δ_{Si}-6.04.

Synthesis of $[\{(Me_2N)_2Hf(\mu_2\text{-}NSiEt_3)\}_2]$ (6). A stirred toluene (20 mL) solution of Et_3SiNH_2 (0.52 g, 4.0 mmol) was treated with a toluene (30 mL) solution of $Hf(NMe_2)_4$ (1.42 g, 4.0 mmol). After stirring for 24 h, volatiles were removed *in vacuo*. Recrystallization of the residue from hexane at −28 °C afforded $[\{(Me_2N)_2Hf(\mu_2\text{-}NSiEt_3)\}_2]$ (**6**) as colorless crystals. Due to an observed high solubility of **12** within hexane at room temperature, crystals were isolated at −20 °C using a NaCl ice bath. Yield: 0.30 g, 19%. Analysis, found (calcd for $C_{20}H_{54}Hf_2N_6Si_2$): C, 29.9 (30.3); H, 6.8 (6.9); N, 10.2 (10.6)%. ^1H NMR (300 MHz, C_6D_6): δ_H 3.05 (s, 4H, NMe_2), 1.09 (t, 3H, CH_2CH_3, $^3J_{CH2\text{-}CH3}$ 7.5), 0.56 (q, 2H, CH_2CH_3, $^3J_{CH2\text{-}CH3}$ 7.5). $^{13}C\{^1H\}$ NMR (75.5 MHz, C_6D_6): δ_C 42.1 (NMe_2), 8.74 (CH_2CH_3), 7.58 (CH_2CH_3,). ^{29}Si NMR (99.35 MHz, C_6D_6): δ_{Si} −4.87.

Synthesis of $[\{(Me_2N)_2Ti(\mu_2\text{-}NSi^tBuMe_2)\}_2]$ (7). A stirred hexane (40 mL) solution of $^tBuMe_2SiNH_2$ (1.60 g, 12.2 mmol) was treated with a hexane (60 mL) solution of $Ti(NMe_2)_4$ (2.74 g, 12.2 mmol). After stirring for 24 h, volatiles were removed *in vacuo*. Recrystallization of the residue from hexane at −28 °C yielded

dx.doi.org/10.1021/ic2015644 | Inorg. Chem. 2011, 50, 12053−12063

$[\{(Me_2N)_2Ti(\mu_2\text{-}NSi^tBuMe_2)\}_2]$ (**7**) as orange crystals. Yield: 2.23 g, 69%. Analysis, found (calcd for $C_{20}H_{54}N_6Si_2Ti_2$): C, 45.4 (45.3); H, 10.1 (10.3), N 15.9 (15.8)%. ^{1}H NMR (300 MHz, C_6D_6): δ_H 3.32 (s, 4H, NMe_2); 0.98 (s, 3H, Si^tBu), 0.15 (s, 2H, SiMe). $^{13}C\{^1H\}$ NMR (75.5 MHz, C_6D_6): δ_C 45.6 (NMe_2), 26.5 ($C(Me)_3$), 18.6 ($C(Me)_3$), −0.70 ($SiMe_2$). ^{29}Si NMR (99.35 MHz, C_6D_6): δ_{Si} −1.07.

Synthesis of $[\{(Me_2N)_2Zr(\mu_2\text{-}NSi^tBuMe_2)\}_2]$ (8). A stirred hexane (15 mL) solution of $^tBuMe_2SiNH_2$ (0.52 g, 4.0 mmol) was treated with a hexane (25 mL) solution of $Zr(NMe_2)_4$ (1.07 g, 4.0 mmol). After stirring for 24 h, volatiles were removed *in vacuo*. Recrystallization of the residue from hexane at −28 °C yielded $[\{(Me_2N)_2Zr(\mu_2\text{-}NSi^tBuMe_2)\}_2]$ (**8**) as colorless crystals. Yield: 0.83 g, 67%. Analysis, found (calcd for $C_{20}H_{54}N_6Si_2Zr_2$): C, 38.6 (38.9); H, 8.9 (8.8); N, 13.8 (13.6) %. ^{1}H NMR (300 MHz, C_6D_6): δ_H 3.10 (s, 4H, NMe_2), 1.00 (s, 3H, Si^tBu), 0.14 (s, 2H, SiMe). $^{13}C\{^1H\}$ NMR (75.5 MHz, C_6D_6): δ_C 42.39 (NMe_2), 26.21 ($C(Me)_3$), 18.04 ($C(Me)_3$), −0.89 ($SiMe_2$). ^{29}Si NMR (99.35 MHz, C_6D_6): δ_{Si} −7.03.

Synthesis of $[\{(Me_2N)_2Hf(\mu_2\text{-}NSi^tBuMe_2)\}_2]$ (9). A stirred hexane (15 mL) solution of $^tBuMe_2SiNH_2$ (0.26 g, 2.0 mmol) was treated with a hexane (25 mL) solution of $Hf(NMe_2)_4$ (0.71 g, 2.0 mmol). After stirring for 24 h, volatiles were removed *in vacuo*. Recrystallization of the residue from hexane at −28 °C yielded $[\{(Me_2N)_2Hf(\mu_2\text{-}NSi^tBuMe_2)\}_2]$ (**9**) as colorless crystals. Yield: 0.27 g, 34%. Analysis, found (calcd for $C_{20}H_{54}Hf_2N_6Si_2$): C, 30.1 (30.3); H, 6.7 (6.9); N, 10.2 (10.6)%. ^{1}H NMR (300 MHz, C_6D_6): δ_H 3.14 (s, 4H, NMe_2), 1.00 (s, 3H, Si^tBu), 0.12 (s, 2H, SiMe). $^{13}C\{^1H\}$ NMR (75.5 MHz, C_6D_6): δ_C 42.04 (NMe_2), 26.14 ($C(Me)_3$), 18.20 ($C(Me)_3$), −0.75 ($SiMe_2$). ^{29}Si NMR (99.35 MHz, C_6D_6): δ_{Si} −5.0.

Synthesis of $[\{(Me_2N)_2Ti(\mu_2\text{-}NSi[NMe_2]_3)\}_2]$ (10). A stirred hexane (60 mL) solution of $(Me_2N)_3SiNH_2$ (11.26 g, 64.0 mmol) was treated with a hexane (40 mL) solution of $Ti(NMe_2)_4$ (14.35 g, 64.0 mmol). After stirring for 24 h, volatiles were removed *in vacuo*. Recrystallization of the residue from hexane at −28 °C yielded $[\{(Me_2N)_2Ti(\mu_2\text{-}NSi[NMe_2]_3)\}_2]$ (**10**) as orange crystals. Yield: 10.95 g, 55%. Analysis, found (calcd for $C_{20}H_{60}N_{12}Si_2Ti_2$): C, 38.1 (38.7); H, 9.7 (9.7); N, 27.2 (27.1)%. ^{1}H NMR (300 MHz, C_6D_6): δ_H 3.29 (s, 2H, $Ti(NMe_2)_2$), 2.56 (s, 3H, $Si(NMe_2)_3$). $^{13}C\{^1H\}$ NMR (75.5 MHz, C_6D_6): δ_C 45.0 (Ti-NMe_2), 38.1 (Si-NMe_2). ^{29}Si NMR (99.35 MHz, C_6D_6): δ_{Si} −49.5.

Synthesis of $[\{(Me_2N)_2Zr(\mu_2\text{-}NSi[NMe_2]_3)\}_2]$ (11). A stirred hexane (20 mL) solution of $(Me_2N)_3SiNH_2$ (0.88 g, 5.0 mmol) was treated with a hexane (20 mL) solution of $Zr(NMe_2)_4$ (1.34 g, 5.0 mmol). After stirring for 24 h, the volume was then reduced under reduced pressure. Crystallization from the reaction solution at −28 °C yielded $[\{(Me_2N)_2Zr(\mu_2\text{-}NSi[NMe_2]_3)\}_2]$ (**11**) as colorless crystals. Yield: 1.10 g, 62%. Analysis, found (calcd for $C_{20}H_{60}N_{12}Si_2Zr_2$): C, 33.8 (34.0); H, 8.8 (8.6); N, 23.9 (23.8)%. ^{1}H NMR (300 MHz, C_6D_6): δ_H 3.01 (s, 2H, $Zr(NMe_2)_2$), 2.62 (s, 3H, $Si(NMe_2)_3$). $^{13}C\{^1H\}$ NMR (75.5 MHz, C_6D_6): δ_C 42.7 (Zr-NMe_2), 40.0 (Si-NMe_2). ^{29}Si NMR (99.35 MHz, C_6D_6): δ_{Si} −48.0.

Synthesis of $[\{(Me_2N)_2Hf(\mu_2\text{-}NSi[NMe_2]_3)\}_2]$ (12). A stirred hexane (20 mL) solution of $(Me_2N)_3SiNH_2$ (0.88 g, 5.0 mmol) was treated with a hexane (20 mL) solution of $Hf(NMe_2)_4$ (1.77 g, 5.0 mmol). After stirring for 24 h, the volume was then reduced under reduced pressure. Crystallization from the reaction solution at −28 °C yielded $[\{(Me_2N)_2Hf(\mu_2\text{-}NSi[NMe_2]_3)\}_2]$ (**12**) as colorless crystals. Yield: 1.48 g, 67%. Analysis, found (calcd for $C_{20}H_{60}Hf_2N_{12}Si_2$): C, 27.1 (27.2); H, 6.8 (6.9); N, 19.3 (19.1)%. ^{1}H NMR (300 MHz, C_6D_6): δ_H 3.02 (s, 2H, $Hf(NMe_2)_2$), 2.60 (s, 3H, $Si(NMe_2)_3$). $^{13}C\{^1H\}$ NMR (75.5 MHz,C_6H_6): δ_C 43.6 (Hf-NMe_2), 40.9 (Si-NMe_2). ^{29}Si NMR (99.35 MHz, C_6D_6): δ_{Si} −45.0.

Crystallography. Experimental details relating to the single-crystal X-ray crystallographic studies are summarized in Table 1. For all structures, data were collected on a Nonius Kappa CCD diffractometer at 150(2) K using Mo Kα radiation (λ = 0.71073 Å). The structure solution was followed by full-matrix least-squares refinement and was performed using the WinGX-1.70 suite of programs.[28] Corrections for absorption (semiempirical) were made in all cases.

Materials Chemistry. TGA analysis of the complexes was performed at SAFC Hitech, Bromborough, United Kingdom, using a Shimadzu TGA-51 Thermogravimetric Analyzer. Data points were collected every second at a ramp rate of 20 °C min^{-1} in a flowing (50 mL min^{-1}) N_2 stream.

Film depositions were carried out at atmospheric pressure in a laminar flow, cold-wall reactor containing a graphite heating block on which the substrate is situated.[29] The precursors were injected as a solution into a glass flask sitting in an ultrasonic nebulizer, located just before the reactor chamber. Prior to injecting the precursor, the chamber was loaded with the glass substrate and heated under a flow of nitrogen (1.2 L/min) to the required temperature at a rate of 10 °C/min before allowing it to equilibrate for at least 30 min. The precursor was then injected and the nebulizer started to begin the deposition. After each deposition, the films were allowed to cool slowly at a rate of 1 °C/min under a flow of nitrogen. The glass substrates used were glass microscope slides and were etched for 24 h in H_2SO_4/HNO_3 (1:1) and then rinsed with deionized water and acetone before loading into the chamber.

RESULTS AND DISCUSSION

Synthesis and Structures. Reaction of a substituted silylamine $R^1R^2R^3SiNH_2$ with $M(NMe_2)_4$ (M = Ti, Zr, Hf) in an equimolar ratio afforded the metal silylamides **1**−**12** (eq 1);[30] the reaction medium was either toluene or hexane:

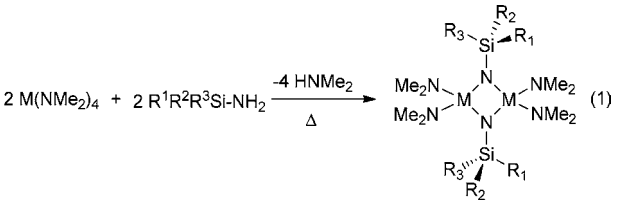

(1)

	Ph_3Si	Et_3Si	$^tBuMe_2Si$	$(Me_2N)_3Si$
Ti	**1**	**4**	**7**	**10**
Zr	**2**	**5**	**8**	**11**
Hf	**3**	**6**	**9**	**12**

All of the titanium compounds (**1**, **4**, **7**, and **10**) were orange, while the remaining zirconium and hafnium compounds were colorless or white. Yields were in the range 34−69%, save **5** and **6** (12 and 19%, respectively) which were particularly soluble in hexane. All of the compounds were notably sensitive to air and moisture.

^{1}H NMR data for **1**−**3** in C_6D_6 show a singlet at *ca.* 2.80 ppm due to the NMe_2 groups, which integrate 12:15 with respect to the Ph_3Si function, implying the elimination of two equivalents of $HNMe_2$ from the precursor metal complex, $M(NMe_2)_4$. In addition, the spectrum of **3** shows the presence of a singlet resonance at 1.60 ppm integrating to 6H, consistent with a molecule of $HNMe_2$ coordinated to one metal center. The associated NH resonance is not observed in the ^{1}H NMR spectrum.

Although coordination of an additional $\{HNMe_2\}$ unit to the dimer system renders the molecule unsymmetrical, the observation of only a single Hf-NMe_2 signal implies significant fluxionality within the coordination sphere. Variable temperature NMR experiments were performed on samples of **3** in both deuterated toluene (d_8-C_7H_8) and deuterated tetrahydrofuran (d_8-THF) in an attempt to elucidate the fluxional processes **3** experiences in solution. Spectra were recorded at intervals over the temperature range 182−298 K. While in both solvent systems fluxional processes were not frozen-out, on

dx.doi.org/10.1021/ic2015644 | *Inorg. Chem.* 2011, 50, 12053−12063

Table 1. Crystal Data and Structure Refinement for 1−4 and 7−12

	1	2	3	4	7	8	9	10	11	12
formula	$C_{44}H_{54}N_6Si_2Ti_2$	$C_{44}H_{54}N_6Si_2Zr_2$	$C_{60}H_{77}N_7Si_2Hf_2$	$C_{20}H_{54}N_6Si_2Ti_2$	$C_{20}H_{54}N_6Si_2Ti_2$	$C_{20}H_{54}N_6Si_2Zr_2$	$C_{20}H_{54}N_6Si_2Hf_2$	$C_{20}H_{60}N_{12}Si_2Ti_2$	$C_{20}H_{60}N_{12}Si_2Zr_2$	$C_{20}H_{60}N_{12}Si_2Hf_2$
fw	1637.82	905.55	1309.45	530.67	530.67	617.31	791.85	620.78	353.71	881.96
cryst syst	monoclinic	monoclinic	triclinic	monoclinic	monoclinic	monoclinic	monoclinic	triclinic	monoclinic	monoclinic
space group	$P2_1/c$	$P2_1/c$	$P\bar{1}$	$P2_1/n$	$P2_1/n$	$P2_1/n$	$P2_1/n$	$P\bar{1}$	C_2/c	$P2_1/n$
a (Å)	13.0630(2)	9.5700(1)	11.4930(2)	10.6660(3)	9.9270(2)	9.9900 (2)	9.9830 (2)	8.3630(2)	17.1910(2)	8.9930 (2)
b (Å)	1281602(2)	11.4540(1)	14.3830(2)	12.7800(3)	13.3320(3)	13.6030(2)	13.5510(2)	10.5940(2)	12.7470(2)	13.9280(2)
c (Å)	18.0421(3)	20.2050(2)	18.4350(4)	11.5560(3)	11.6030(3)	11.6610(2)	11.6860(2)	10.7400(2)	15.7610(2)	13.7290(2)
α (deg)			85.947(1)					68.206(1)		
β (deg)	133.606(1)	98.163(1)	80.433(1)	97.463(1)	91.029(1)	90.837(1)	90.899(1)	72.139(1)	90.141(1)	101.626(1)
γ (deg)			82.270(1)					78.303(1)		
U/Å	2187.16(6)	2192.33(4)	2974.04(9)	1561.87(7)	1535.37(6)	1584.49(6)	1580.68(5)	836.68(3)	3453.76(8)	1684.34(6)
Z	2	2	2	2	2	2	2	2	4	2
ρ_{calcd} mg/m^{-3}	1.243	1.372	1.462	1.128	1.148	1.294	1.664	1.232	1.360	1.739
μ(Mo Kα), mm^{-1}	0.457	0.567	3.571	0.605	0.615	0.750	6.656	0.579	0.702	6.260
F(000)	864	936	1316	576	576	648	776	336	1488	872
cryst size, mm	0.25/0.25/0.2	0.2/0.15/0.13	0.25/0.20/0.10	0.25/0.20/0.20	0.15/0.15/0.10	0.17/0.13/0.10	0.20/0.17/0.10	0.20/0.10/0.08	0.20/0.10/0.10	0.12/0.10/0.10
Θ range (deg)	3.78−30.2	3.27−30.49	8.52−30.52	7.86−30.52	7.86−30.50	7.87−28.31	7.86−28.31	3.42−30.55	3.90−30.50	3.73−30.51
reflns collected	41005	34645	53103	28631	32777	26053	25625	16226	35910	35032
independent reflns [R(int)]	6078 [0.0990]	6664 [0.0526]	17220 [0.0463]	4635 [0.0422]	4571 [0.0926]	3851 [0.0306]	3847 [0.0421]	5016 [0.0407]	5230 [0.0439]	5116 [0.0711]
reflns obsd [$I > 2\sigma(I)$]	3593	5835	11509	3688	3103	3559	3569	3758	4453	3904
max, min transmn	0.9142, 0.8943	0.9299, 0.8950	0.7166, 0.4689	0.8886, 0.8635	0.9411, 0.9134	0.9288, 0.8831	0.5558, 0.3495	0.9552, 0.8930	0.9331, 0.8723	0.5733, 0.5204
data/restraints/params	6078/0/248	6664/0/248	17220/0/559	4635/0/143	4571/0/145	3851/0/145	3847/0/145	5016/0/173	5230/0/173	5116/0/174
final $R1$ (wR_2) [$I > 2\sigma(I)$]	0.0528 (0.1154)	0.0273 (0.0694)	0.0387 (0.0833)	0.0468 (0.1164)	0.0392 (0.0796)	0.0188 (0.0494)	0.0181 (0.0444)	0.0374 (0.0890)	0.0242 (0.0582)	0.0277 (0.0481)
final $R1$ (wR_2) (all data)	0.1244 (0.1400)	0.0339 (0.0734)	0.0775 (0.0956)	0.0635 (0.1266)	0.0823 (0.0872)	0.0214 (0.0512)	0.0208 (0.0457)	0.0607 (0.0990)	0.0328 (0.0616)	0.0508 (0.0527)
largest diff. peak and hole, eÅ^{-3}	0.618, −0.604	0.564, −0.533	1.382, −0.942	0.558, −0.386	0.302, −0.427	0.393, −0.418	1.014, −1.318	0.580, −0.493	0.356, −0.622	0.819, −1.587

dx.doi.org/10.1021/ic2015644|Inorg. Chem. 2011, 50, 12053−12063

changing the solvent system from C_6D_6 to d_8-THF, there are two notable changes in the spectrum: first, the singlet resonance attributed to the additional coordinated {$HNMe_2$} group, observed in C_6D_6 at 1.60 ppm, is significantly shifted in d_8-THF to 2.39 ppm, appearing as a doublet (^3J = 6.2 Hz). The second change in the spectra is the appearance of a broad singlet resonance at 0.69 ppm integrating to 1H, also attributed. to the {$HNMe_2$} group.

The ^{1}H NMR spectra of the remaining compounds **4**−**12** are unexceptional and follow the same pattern as **1**−**3**; that is, they establish the elimination of two moles of $HNMe_2$ and the formation of the imide $(Me_2N)_2M{=}NSiR_3$. None of the other hafnium species, **6**, **9**, and **12**, have evidence of coordinated amine in their NMR spectra.

X-ray diffraction reveals that the formally imido species $(Me_2N)_2M{=}NSiR_3$ are all dimers with μ_2-$NSiR_3$ groups bridging two metals. The structures of **2** (Figure 1) and **9** (Figure 2) are shown as typical, while data for **1**, **4**, **7**, and **8** (which are structurally very similar) are available as Supporting Information. Selected geometric data for the compounds analyzed are given in Table 2 for comparison. Both **2** and **9** are centrosymmetric about the midpoint of a planar M_2N_2 ring and incorporate tetrahedral metal (Zr, Hf) centers. The imido nitrogen [N(3)] bridges the two metal centers in an asymmetric manner for all of the titanium species **1**, **4**, and **7**, but the bridging is essentially symmetrical for both Zr (**2**, **8**) and Hf (**9**) analogues. The geometry within the M_2N_2 ring has a more acute N−M−N angle than that at N, i.e., ∠M−N−M, though again the titanium species differ in having angles separated by *ca.* 8°, while for the heavier analogues the difference is more marked (*ca* 12 −17°). The geometry at all of the metal-bound amino nitrogen atoms N(1) and N(2) is planar (Table 2), though there is some small pyramidalization (*ca.* 3−4° deviation from Σ angles at N = 360°) at the imido N(3) (Figure 3a), similar to that seen in non-silylated compounds such as $[(Me_2N)_2Ti(\mu\text{-}NBu^t)]_2$.[31] This moves the two R_3Si groups out of the M_2N_2 plane in an *anti* arrangement, as predicted theoretically;[32] the exception here is the Zr species **2** (Figure 3b), which is perfectly planar. The Si−N bonds are largely invariant [*ca.* 1.73 Å], save for that in **2** [1.7068(12) Å], which is notably shorter and which seems to correlate with the weak bridging Zr−N(3) interactions. Furthermore, as previously noted, this is the example which is perfectly planar at N(3), which collectively suggests a more significant donation of the imido lone pair to silicon in this compound. This is illustrated in Figure 3, which highlights the relative orientations of the NMe_2 groups with respect to the M_2N_2 ring. In, for example, **1**, one $TiNMe_2$ group [based on N(2)] is not orthogonal to the M_2N_2 plane; thus, the *p* orbital housing the lone pair on this amide is not perfectly oriented for π-bonding with the *d* orbitals on titanium (Figure 3a), resulting in greater involvement of the lone pair on the imino nitrogen in π-bonding within the M_2N_2 ring and consequently a relatively long Si−N(3) bond. Conversely, in **2**, all four Zr-NMe_2 units are oriented closely orthogonal to the M_2N_2 ring, such that the N(p) orbitals maximize their π interactions with the metal leaving the imido nitrogen to enhance its π-bonding toward silicon (Figure 3b). There is, however, no evidence to be found for donation into the σ^* orbital of the relevant Si−C(Ph) in a lengthening of this bond relative to the remaining Si−C(Ph) distances.

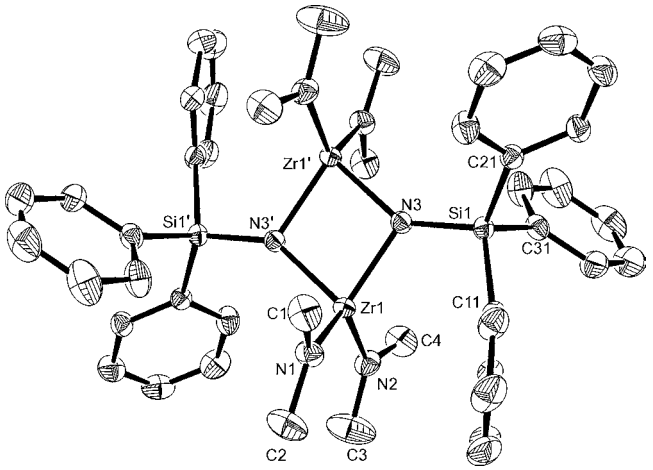

Figure 1. The molecular structure of **2** showing the labeling scheme used in the text and tables. Thermal ellipsoids are at the 50% level. Symmetry operation: 1 − *x*, 1 − *y*, 1 − *z*.

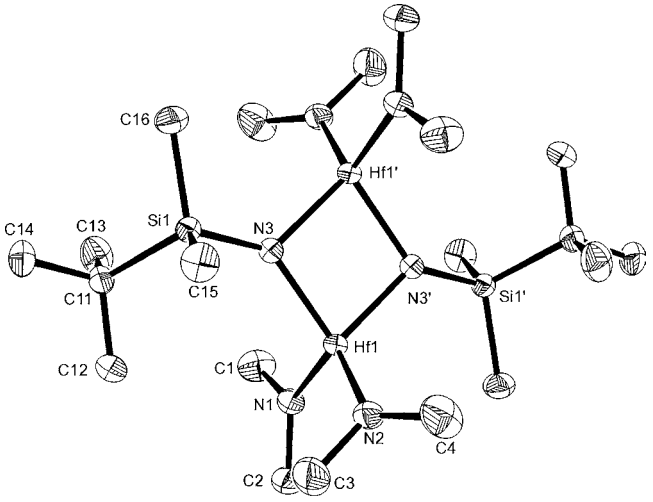

Figure 2. The molecular structure of **9** showing the labeling scheme used in the text and tables. Thermal ellipsoids are at the 50% level. Symmetry operation: 1 − *x*, 1 − *y*, 1 − *z*.

The structure of the hafnium analogue (**3**) is shown in Figure 4 and confirms the presence of a coordinated $HNMe_2$ moiety at Hf(2). Similar complexes possessing a [Hf−N(H)Me_2] moiety have previously been reported by Gao et al.[33] and Hughes et al.[34] The two metals are no longer equivalent, with Hf(1) remaining four-coordinate while Hf(2) is five-coordinate as a result of the donor N(7):→Hf bond *trans* to N(6) [2.442(4) Å]. This has little impact on the remaining Hf−NMe_2 bonds but does induce notable asymmetry into the Hf−N bond lengths in the Hf_2N_2 ring (Table 2). In addition, the geometry about the imido nitrogens N(3,6) is, as in **2**, almost planar, and again the Si−N bonds are shortened [1.714(3), 1.705(3) Å]. Further correlation with the orientation of the Hf-NMe_2 groups with respect to the Hf_2N_2 ring are rendered less clear by virtue of distortions caused by the coordinated $HNMe_2$, but only the amino group based on N(1) is markedly twisted away from the optimum π-bonding orientation (Figure 4).

The most surprising trio of compounds is **10**, **11**, and **12**. Compound **10**, which has been synthesized previously by the reaction of $(Me_2N)_3Si{-}N\{B(NMe_2)_2\}_2$ with $TiCl_2(NMe_2)_2$,[35] adopts a comparable molecular structure to compounds **1**, **2**, **4**, **7**, **8**, and **9** and need not be discussed further. The Zr (**11**) and Hf (**12**) analogues, however, are structurally unique within this

dx.doi.org/10.1021/ic2015644 | *Inorg. Chem.* 2011, 50, 12053−12063

Table 2. Selected Geometric Data for 1−4 and 7−12

	Ti				Zr			Hf		
	1	**4**	**7**	**10**	**2**	**8**	**11**	**3**	**9**	**12**
					bond lengths (Å)					
terminal M−N										
M−N(1)	1.9033(19)	1.9084(18)	1.8984(13)	1.9111(13)	2.0551(14)	2.0595(10)	2.0711(12)	2.041(3)[a]	2.0403(19)	2.051(2)
M−N(2)	1.8889(18)	1.8953(18)	1.9096(13)	1.9081(13)	2.0454(12)	2.0499(11)	2.0604(11)	2.042(3)[a]	2.033(2)	2.056(2)
bridging M-N										
M−N(3)	1.9182(18)	1.8937(16)	1.9089(12)	1.9111(13)	2.0737(11)	2.0700(10)	2.0995(11)	2.050(3)[b]	2.0550(18)	2.138(2)
M−N(3′)	1.9416(17)	1.9448(16)	1.9365(12)	1.9598(13)	2.0783(12)	2.0619(10)	2.0801 (10)	2.121(3)	2.0462(18)	2.039(2)
coordinate M←N							2.5918(11)[c]	2.442(3)[d]		2.484(2)[e]
Si−N(3)	1.7264(18)	1.7311(17)	1.7360(12)	1.7315(13)[f]	1.7068(12)	1.7257(10)	1.6798(10)[g]	1.714(3)	1.728(2)	1.673(2)[i]
								1.705(3)[h]		
					bond angles (deg)					
N(3)−M−N(3′)	86.49(7)	86.60(7)	86.45 (5)	86.54(6)	81.43(5)	82.94(4)	80.50(4)	84.07(12)[j]	83.81(8)	80.41(10)
								80.02(11)		
M−N(3)−M′	93.50(7)	93.40(7)	93.55 (5)	93.46(6)	98.57(5)	97.06(4)	99.50(4)	97.53(13)[k]	96.19(8)	99.59(10)
								98.24(13)		
Σ[N(1)]	359.96(17)	359.96(18)	359.94(12)	359.99 (12)[l]	359.99(13)	359.91(10)	359.99(12)[m]	359.6(4)[n]	359.97(18)	359.9(2)[p]
Σ[N(2)]	359.95(16)	359.88(19)	359.99(13)	359.88 (12)	360.00(13)	359.78(11)	359.02 (13)	360.0(3)[n]	359.90(19)	359.81(2)
Σ[N(3)]	357.58(9)	356.21(9)	356.10(6)	353.30(7)	360.00(6)	357.72(5)	359.73(5)	359.95(15)[q]	357.50(8)	360.00(11)

[a]Hf(2)−N(4), 2.024(3); Hf(2)−N(5), 2.030(3) Å. [b]Hf(2)−(N6), 2.121(3); Hf(2)−N(3), 2.123(3) Å. [c]Zr−N(4). [d]Hf−N(7). [e]Hf−N(4). [f]Other Si−NMe_2: Si(1)−N(4,5,6), respectively, 1.7187 (14), 1.7254 (14), 1.7179 (14) Å, all terminal. [g]Other Si−NMe_2: Si(1)−N(4), 1.7982(12); Si(1)−N(5), 1.7122(12); Si(1)−N(6), 1.7144(13) Å, terminal. [h]Si−N(6). [i]Other Si−NMe_2: Si(1)−N(4), 1.826(3); Si(1)−N(5), 1.719(2); Si(1)−N(4), 1.713(2) Å. [j]N(3)−Hf(1,2)−N(6). [k]Hf(1)−N(3,6)−Hf(2). [l]Σ[Si(N)Me_2] N(4,5,6) ,respectively, 356.59(12), 354.80(12), 356.87(12)°. [m]Σ[Si(N)Me_2] N(5,6) respectively: 355.67(11), 359.78 (12)°. [n]Σ[N(4)]: 360.0(3)°. Σ[N(5)]: 359.8(3)°. [p]Σ[Si(N)Me_2] N(5,6), respectively, 356.0(2), 357.18(2)°. [q]Σ[N(6)]: 359.378(15).

dx.doi.org/10.1021/ic2015644|*Inorg. Chem.* 2011, 50, 12053−12063

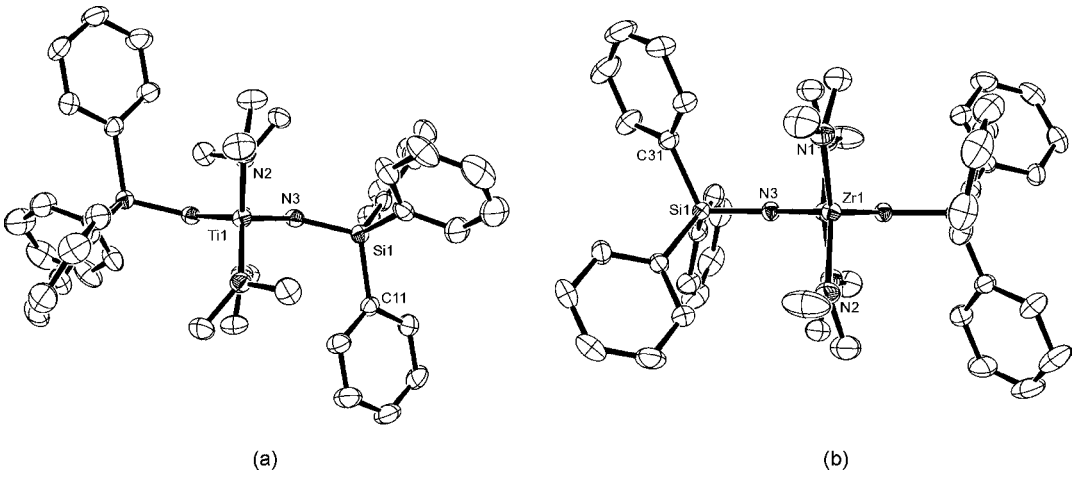

Figure 3. The relative disposition of Ph_3Si groups with respect to the M_2N_2 ring in (a) **1** and (b) **2**.

series of complexes. Both adopt a similar dimeric structure seen in all of the previous examples, based around a central M_2N_2 core (Figures 5 and 6, respectively). However, in both cases, one of the terminal $SiNMe_2$ groups of the $\{Si(NMe_2)_3\}$ ligand also coordinates to the metal *via* an intramolecular N:→M bond [M−N: Zr 2.5918(11); Hf 2.484(2) Å], generating a four-membered MN_2Si ring fused through a common M−N edge with the M_2N_2 ring. Comparable bonding motifs have also been observed in related lithium,[27,36] iron,[37] zinc,[38] hafnium,[39] and zirconium[40] complexes.

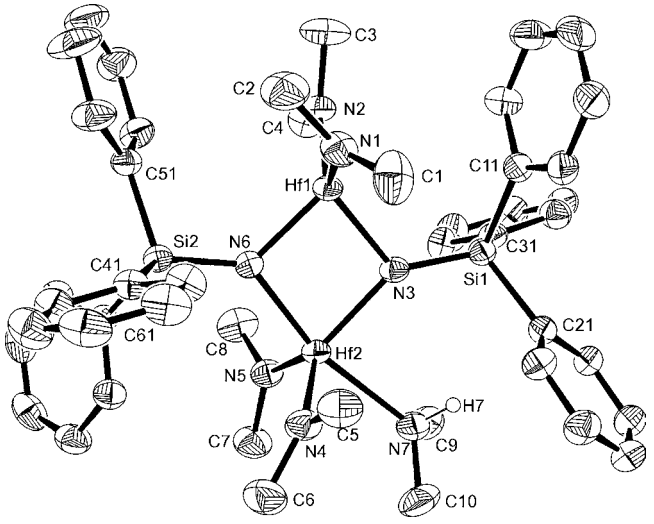

Figure 4. The molecular structure of **3** showing the labeling scheme used in the text and tables. Thermal ellipsoids are at the 40% level.

There are significant structural consequences which result from this intramolecular bonding. First, there is considerable elongation of this Si−N bond [Zr, 1.7982(12); Hf, 1.826(3) Å] in comparison to the other Si−N bonds (all *ca.* 1.71 Å; Table 2). Second, the bridging N(3) is planar, unlike the clear pyramidalization seen in all of the other structures save **3**, discussed above. Associated with this planarity is, again, a shortening of the N(3)−Si bond [Zr, 1.6798 (10); Hf, 1.673(2) Å], suggesting a significant π-interaction between these centers, and a concomitant lengthening of one (Hf) or both (Zr) M−N bonds within the M_2N_2 ring (Table 2). The geometry at the metal in both cases can be described as distorted trigonal bipyramidal.

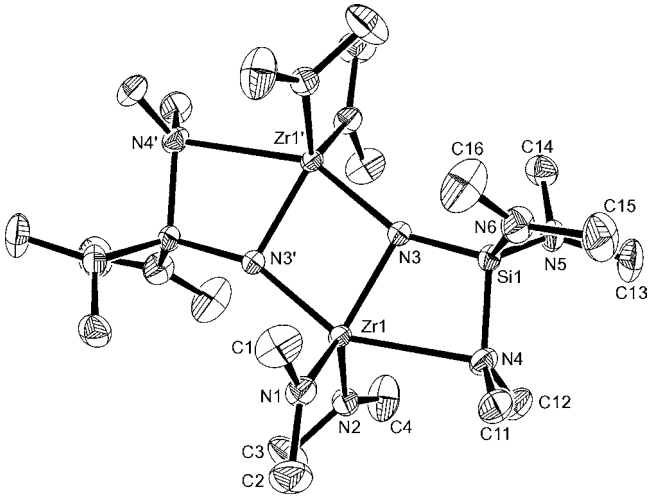

Figure 5. The molecular structure of **11** showing the labeling scheme used in the text and tables. Thermal ellipsoids are at the 50% level. Symmetry operation: $1 - x$, $1 - y$, $1 - z$.

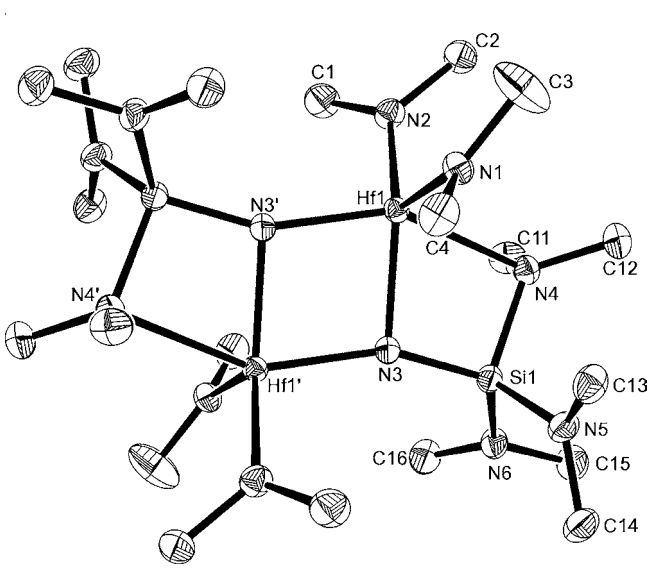

Figure 6. The molecular structure of **12** showing the labeling scheme used in the text and tables. Thermal ellipsoids are at the 50% level. Symmetry operation: $1/2 - x$, $1/2 - y$, $-z$.

dx.doi.org/10.1021/ic2015644 | *Inorg. Chem.* 2011, 50, 12053–12063

Despite the obvious inequivalence of the {Si-NMe_2} groups within **11** and **12** in the solid state, the ^{1}H NMR spectra of the complexes are unexceptional, showing singlet resonances for both the M−NMe_2 and Si−NMe_2 groups, suggesting a significant degree of fluxionality in solution. Attempts to freeze out fluxional process in **11** and **12** using variable-temperature NMR spectroscopy (d_8-C_7D_8, 203−298 K) were unsuccessful.

Materials Chemistry. TGA data for selected complexes are shown in Figure 7; all of the species studied show an early

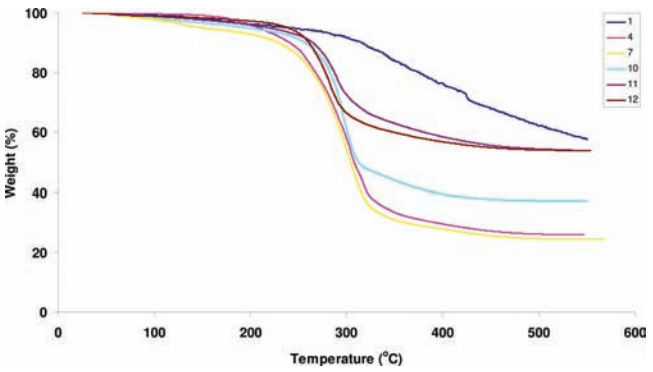

Figure 7. TGA data for **1**, **4**, **7**, **10**−**12**.

onset of decomposition which may be due to a loss of traces of residual solvent. The triphenylsilyl species typified by **1** show a slow decomposition over a wide temperature range and leave a residual mass at 550 °C (54.4%) which is considerably in excess of TiN (15.1%) or TiNSi (22.0%). It would appear that decomposition at this point is far from complete, and these species (**1**−**3**) are not suitable as CVD precursors. The related Et_3Si- and $^tBuMe_2Si$-subsituted titanium species (**4** and **7**, respectively) decompose more rapidly over the range *ca.* 200−350 °C, leaving residues (25.9 and 24.4%) which are close to, but slightly in excess of, the values for TiN (23.4%). The two $(Me_2N)_3SiN$-M species (**10** and **12**) behave similarly, despite the structural differences described earlier. Both species leave a residual mass (*ca.* 37% and 54%, respectively) which is close to the mass calculated for 3MN + $2Si_3N_4$ (M = Ti, 35.0; Hf 54.3%), though this in no way implies that such discrete species are present. Such species could, however, arise from the following reaction:

$$3[(Me_2N)_3SiM(NMe_2)_2]_2 \rightarrow 6MN + 2Si_3N_4 + \text{volatile byproducts}$$

The anomaly in this series is the zirconium analogue (**11**), which has a similar decomposition profile to those of **10** and **12** (Figure 7) but which leaves a residual mass (54%) well in excess of that expected for 3ZrN + $2Si_3N_4$ (43%) and for which no obvious explanation is forthcoming. In all cases, the decomposition products are amorphous, so no further comments can be made about the nature of the residues and, in particular, the presence of insulating phases such as M_3N_4 (M = Zr, Hf) rather than the mononitrides.

Films were deposited by aerosol-assisted CVD (AACVD) using nebulized hexane solutions and a glass substrate temperature of 500 °C. At lower substrate temperatures, low growth rates were observed, and only poorly adherent powdery films were deposited. In appearance, the films are golden with some darkening due to surface carbon contamination (*vide infra*), most notably the films grown from the precursors involving the species $[(Me_2N)_2M(NSiMe_2Bu^t)]_2$ (**7**−**9**). A SEM of the film grown from **4** can be found in the Supporting Information, from which the thickness of the film can be seen to be *ca.* 2 μm, giving an approximate growth rate of 4150 Å min^{-1}.

EDX analysis of the films shows the presence of the appropriate metal, silicon, and the light atoms carbon and oxygen but not nitrogen. However, XPS analysis confirms the presence of all of the expected elements including nitrogen, and depth profiling shows that the silicon is present throughout the film, though in the EDX, an additional signal enhancement from the glass substrate cannot be ruled out.

XPS data at sputter etching times of 0, 30, 60, and 90 s for the films deposited from the three $[(Me_2N)_2M(NSiEt_3)]_2$ species **4** (Ti), **5** (Zr), and **6** (Hf) are shown in Figure 8. Carbon levels are high at the surface, which possibly arises from graphitic carbon deposition, a result of hexane decomposition. At 60 s etching and beyond, the film composition in all cases remains relatively stable within the limits of the measurements, and analytical data at this depth for all of the films examined are given in Table 3.

XPS shows that the metal, nitrogen, silicon, carbon, and oxygen are distributed throughout the films at broadly similar levels irrespective of either the metal or the precursor ligand substituents (Figure 8). For example, there is neither more nitrogen nor less carbon in the films derived from $[(Me_2N)_2M$-$NSi(NMe_2)_3]_2$ (**10** and **12**) in comparison with the remaining $[(Me_2N)_2M(NSiR)_3]_2$ precursors (**4**−**7** and **9**). This suggests a common intermediate in the decomposition process. The atomic percentages must, however, be treated with caution, as XPS preferentially sputters light elements and hence can underestimate the amount of these present. For example, in a study of the films derived from $Ti(NR_2)_4$, XPS consistently overestimated the amount of Ti at the expense of N and C when compared with data obtained from either Rutherford backscattering spectrometry (RBS) or electron microprobe analysis (EMA).[41] In comparison with TiN/C/O films derived from $Ti(NR_2)_4$ by APCVD, the presence of large amounts of silicon in the films produced in this work (Si/M 0.47−0.99) seems to be at the expense of nitrogen, where the M/N of

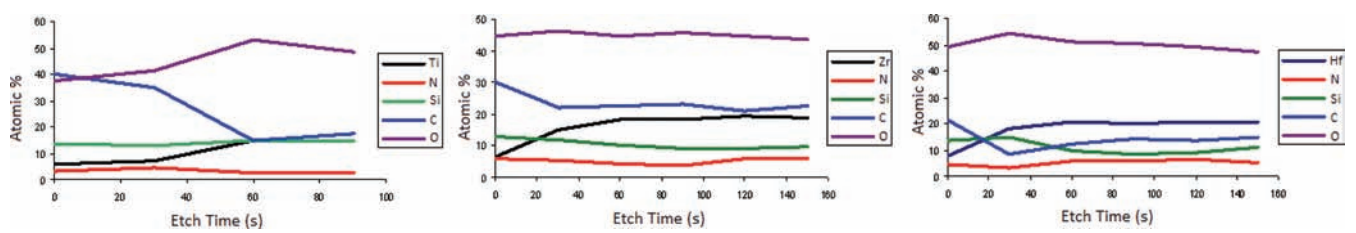

Figure 8. XPS data for **4**−**6** at sputter-etching times of 0, 30, 60, 90 (**4**), 120, and 150 s (**5**, **6**).

dx.doi.org/10.1021/ic2015644 | *Inorg. Chem.* 2011, 50, 12053−12063

Table 3. Film Composition Derived from XPS after 60 s Sputter Etching

	M (at %)	N (at %)	Si (at %)	C (at %)	O (at %)	N/M	Si/M	C/M	O/M
4	14.90	2.72	14.79	14.67	52.92	0.18	0.99	0.98	3.55
7	17.57	4.99	16.53	12.38	48.52	0.28	0.94	0.70	2.76
10	18.26	4.42	14.90	9.92	52.50	0.24	0.82	0.54	2.88
5	18.42	4.13	10.14	22.47	44.83	0.22	0.55	1.22	2.43
6	20.34	5.84	9.59	12.45	50.75	0.29	0.47	0.61	2.50
9	19.97	3.77	13.90	16.30	46.07	0.19	0.70	0.82	2.31
12	20.13	6.07	10.92	14.45	48.45	0.30	0.54	0.72	2.41

0.18−0.29 is about half that in the former case (by XPS; Ti/N *ca.* 0.6−0.9).[41] While Ti/N/C films are known to easily oxidize from traces of O_2/H_2O in the carrier gas or adsorbed onto the reactor walls, the level of oxygen incorporation in all of the films reported here is higher than in previously reported films derived from non-silylated precursors, albeit by APCVD rather than our aerosol delivery method. It is possible that oxygen present in the aerosol-generating solvent contributes to this observation. Interestingly, quaternary titanium silicon oxynitride thin films, TiSiNO, have been investigated as promising candidates for next-generation diffusion barrier materials,[42] while the use of hafnium silicon oxynitride, HfSiNO, as a potential gate material in *n*-MOSFETs has been reported by Kamiyama et al.[43]

The XPS binding energies of the relevant elements are given in Table 4 for the composition at 60 s of etching time, which is typical of the film bulk. The presence of carbon has been noted by others in films formed by the APCVD of $Ti(NR_2)_4$, where both metal-bound and organic carbon (i.e., bonded to light elements such as N, O, H, etc.) were identified by XPS binding energies.[41] Analysis of the XPS 1s C region of the spectra derived from all films reported here shows a peak at a binding energy of *ca.* 284 eV consistent with organic carbon. At the surface this peak is relatively sharp, from carbon arising from natural sample contamination or from decomposition of the aerosol solvent used in the AACVD process. At a depth of 60 s sputtering, the peak becomes extremely broad (typically *ca.* 5 eV full width) and extends to lower binding energies, suggesting the additional presence of carbon, bonded to the metal, within the film (TiC = 281.5; ZrC = 281.1; HfC = 280.8 eV);[44] in the case of the film derived from **12**, two clearly separate 1s C binding energies of 284.9 and 282.4 eV are visible and support this interpretation.

Table 4. XPS Binding Energies (eV) for the Elements in the Deposited Films[a]

	M[b]	Si	C	N	O
4	458.5, 463.4	102.6	284.8	396.9	531.8
7	458.1, 463.1	102.8	284.1	397.1	531.5
10	458.3, 464.1	102.7	283.5	397.1	531.4
5	182.7, 184.9	101.9	284.2	396.9	531.0
6	17.1, 18.7	101.7	284.8	396.8	531.0
12	17.4, 18.9	102.1	284.9, 282.4	396.4	530.9

[a]Based on 2p $Ti_{3/2,1/2}$, 3d $Zr_{5/2,3/2}$, 4f $Hf_{7/2,5/2}$, 2p Si(unresolved), 1s C, 1s N, 1s O. [b]**4**, **7**, **10**, M = Ti; **5**, M = Zr; **6**, **9**, **12**, M = Hf.

The 2p Si binding energies fail to resolve the $Si_{3/2,1/2}$ components, suggesting that a range of silicon environments are present. The average binding energies (101.7−102.8 eV) are too low to be attributable to SiO_2 alone (*ca.* 103.5 eV)[45] and are more in keeping with Si−N at 102 eV.[45] For comparison, HfSiON environments have been assigned binding energies of *ca.* 101.6 eV.[46] It would seem, therefore, that the silicon is largely bonded to nitrogen, rather than oxygen, in these films.

The 1s N XPS signals are relatively weak, consistent with the quantitative analysis, and are at binding energies typical of N^{3-} (*ca.* 397 eV).[47] For comparison, Si−N (397.3 eV),[46] Ti−N (396.7 eV),[48] Zr−N (397.3 eV),[49] and Hf−N (396.1 eV)[46] environments all give similar 1s N binding energies; there is no evidence for oxidized nitrogen (N−O) at binding energies of *ca.* 400 eV.[45,47]

The large amounts of oxygen in the films all seem to be associated with the Ti, Zr, or Hf, based on binding energies. For example, the 1s O spectra are all essentially the same for all films studied (*ca.* 531 eV) and are typical of M−O (M = Si, Ti, Zr, Hf).[48a,50] The 2p $Ti_{3/2,1/2}$ binding energies in the films derived from **4**, **7**, and **10** (*ca.* 458, 463 eV) compare closest with those for TiO_2[47,48] rather than Ti−N (*ca.* 455, 461 eV)[47,48] or TiO/N (*ca.* 456, 461 eV),[47,48] though the 1s N binding energies suggest that at least some Ti−N environments are also present. Similarly, the 3d $Zr_{5/2}$ binding energies in the film formed from **5** (182.7 eV) can be compared with ZrO_2 (183.1 eV), ZrO/N (182 eV), and Zr−N (180.1 eV),[47] again consistent with both dominant Zr−O and minority Zr−N environments. There is no evidence for any Zr−Si centers with 3d $Zr_{5/2}$ binding energy *ca.* 179 eV.[50] Finally, the films derived from the hafnium precursors **6**, **9**, and **12** all have 4f $Hf_{7/2}$ binding energies (*ca.* 17.3 eV), typical of HfO_2 (*ca.* 16.8 − 17.2 eV),[46,50,51] though some reports assign similar values to Hf−O environments within HfSiON;[46,52] significant contributions from Hf−N or Hf−Si (typically *ca.* 16.1 and 14.3 eV, respectively)[46,50] can be ruled out.

CONCLUSIONS

A range of Ti, Zr, and Hf silylimides have been prepared and structurally characterized. Representative compounds have been used to deposit amorphous films containing metal, silicon, and nitrogen along with both carbon and oxygen, with all elements distributed throughout the films. The high levels of the latter two elements may be a result of the aerosol-assisted CVD process used to deposit the films. Work directed toward the minimization of the oxygen contaminant in the thin films using different deposition conditions, including the use of ammonia as a coreagent, is under way, the results of which will form the basis of future publications.

ASSOCIATED CONTENT

Supporting Information

Visual appearance of the films deposited from titanium precursors **4**, **7**, and **10**; zirconium precursors **5** and **8**; and hafnium precursors **6**, **9**, and **12**. SEM of the film derived from precursor **4**. Crystallographic information in CIF format. This material is available free of charge via the Internet at http://pubs.acs.org.

dx.doi.org/10.1021/ic2015644 | *Inorg. Chem.* 2011, 50, 12053−12063

AUTHOR INFORMATION

Corresponding Author

*E-mail: a.l.johnson@bath.ac.uk.

ACKNOWLEDGMENTS

We thank Dr. D. J. Morgan (Cardiff University) and the EPSRC (through the "Access to Materials Research Equipment" initiative) for the XPS data.

REFERENCES

(1) International Technology Roadmap for Semiconductors, 2009 Edition. http://www.itrs.net (accessed Oct 2011).

(2) (a) Gupta, T. *Copper Interconect Technology*; Springer: New York, 2009. (b) Eisenbraun, E.; Upham, A.; Dash, R.; Zeng, W. X.; Hoefnagels, J.; Lane, S.; Anjum, D.; Dovidenko, K.; Kaloyeros, A.; Arkles, B.; Sullivan, J. J. *J. Vac. Sci. Technol. B* **2000**, *18*, 2011.

(3) (a) Bracht, H. *Mat. Sci. Semicon. Proc.* **2004**, *7*, 113. (b) Bracht, H.; Stolwijk, N. A.; Mehrer, H. *Phys. Rev. B* **1991**, *43*, 14465.

(4) (a) Carmalt, C. J.; Newport, A.; Parkin, I. P.; Mountford, P.; Sealey, A. J.; Dubberley, S. R. *J. Mater. Chem.* **2003**, *13*, 84. (b) Carmalt, C. J.; Newport, A. C.; Parkin, I. P.; White, A. J. P.; Williams, D. J. *J. Chem. Soc., Dalton Trans.* **2002**, 4055. (c) Parkin, I. P.; Newport, A.; Carmalt, C. J.; O'Neill, S. A. *J. Mater. Chem.* **2002**, *12*, 1906. (d) Carmalt, C. J.; Cowley, A. H.; Culp, R. D.; Jones, R. A.; Sun, Y. M.; Fitts, B.; Whaley, S.; Roesky, H. W. *Inorg. Chem.* **1997**, *36*, 3108. (e) Lewkebandara, T. S.; Sheridan, P. H.; Heeg, M. J.; Rheingold, A. L.; Winter, C. H. *Inorg. Chem.* **1994**, *33*, 5879. (f) Winter, C. H.; Lewkebandara, T. S.; Proscia, J. W.; Rheingold, A. L. *Inorg. Chem.* **1994**, *33*, 1227. (g) Winter, C. H.; Sheridan, P. H.; Lewkebandara, T. S.; Heeg, M. J.; Proscia, J. W. *J. Am. Chem. Soc.* **1992**, *114*, 1095.

(5) (a) Fischer, R. A.; Baunemann, A.; Kim, Y.; Winter, M. *Dalton Trans.* **2006**, 121. (b) Fix, R.; Gordon, R. G.; Hoffman, D. M. *Chem. Mater.* **1991**, *3*, 1138. (c) Musgrave, C.; Somani, S.; Mukhopadhyay, A. *J. Phys. Chem. C* **2011**, *115*, 11507. (d) Hoffman, D. M.; Lehn, J. S. B. M.; van der Heide, P.; Wang, Y. Q.; Suh, S. *J. Mater. Chem.* **2004**, *14*, 3239. (e) Carmalt, C. J.; Hasan, P.; Potts, S. E.; Palgrave, R. G.; Davies, H. O. *Polyhedron* **2008**, *27*, 1041. (f) Mountford, P.; Dubberley, S. R.; Evans, S.; Boyd, C. L. *Dalton Trans.* **2005**, 1448.

(6) (a) Kaloyeros, A. E.; Eisenbraun, E. *Annu. Rev. Mater. Sci.* **2000**, *30*, 363. (b) Rawal, S.; Norton, D. P.; Ajmera, H.; Anderson, T. J.; McElwee-White, L. *Appl. Phys. Lett.* **2007**, *90*, 051913. (c) Winkelmann, A.; Cairney, J. M.; Hoffman, M. J.; Martin, P. J.; Bendavid, A. *Surf. Coat. Technol.* **2006**, *200*, 4213. (d) Chang, C.-L.; Lin, C.-T.; Tsai, P.-C.; Ho, W.-Y.; Liu, W.-J.; Wang, D.-Y. *Surf. Coat. Technol.* **2008**, *202*, 5516.

(7) Winter, C. H. *Aldrichimica Acta* **2000**, *33*, 3.

(8) Hübner, R.; Hecker, M.; Mattern, N.; Hoffmann, V.; Wetzig, K.; Heuer, H.; Wenzel, C. H.; Engelmann, H.-J.; Gehre, D.; Zschech, E. *Thin Solid Films* **2006**, *500*, 259.

(9) Jun, K.; Shimogaki, Y. *Sci. Technol. Adv. Mater.* **2004**, *5*, 549.

(10) Guo, C. T.; Lee, D.; Chen, P. C. *Appl. Surf. Sci.* **2008**, *254*, 3130.

(11) Shalish, I.; Shapira, Y. *J. Vac. Sci. Technol., B: Microelectron. Nanometer Struct.-Process., Meas., Phenom.* **1999**, *17*, 166.

(12) Sun, S. C.; Yap, H. K.; Chen, C. A.; Lin, P. *Solid-State and Integrated-Circuit Technology, Proceedings*; 2001.

(13) Vomiero, A.; Boscolo Marchi, E.; Quaranta, A.; Della Mea, G.; Brusa, R. S.; Mariotto, G.; Felisari, L.; Frabboni, S.; Tonini, R.; Ottaviani, G.; Mattei, G.; Scandurra, A.; Puglisi, O. *J. Appl. Phys.* **2007**, *102*, 033505.

(14) Wen, H. C.; Alshareef, H. N.; Luan, H.; Choi, K.; Lysaght, P.; Harris, H. R.; Huffman, C.; Brown, G. A.; Bersuker, G.; Zeitzoff, P.; Huff, H.; Majhi, P.; Lee, B. H. *Symposium on VLSI Technology, Digest of Technical Papers*; 2005; p 46.

(15) Sandu, C. S.; Benkahoul, M.; Sanjinés, R.; Lévy, F. *Surf. Coat. Technol.* **2006**, *201*, 2897.

(16) Aouadi, S. M.; Namavar, F.; Gorishnyy, T. Z.; Rohde, S. L. *Surf. Coat. Technol.* **2002**, *160*, 145.

(17) (a) Prindle, C.; Brennan, B.; Denning, D.; Shahvandi, I.; Guggilla, S.; Chen, L.; Marcadal, C.; Deyo, D.; Bhandary, U. *Proceedings of the IEEE International Interconnect Technology Conference*; 2002; p 182. (b) Perez-Mariano, J.; Lau, K.-H.; Sanjurjo, A.; Caro, J.; Casellas, D.; Colominas, C. *Surf. Coat. Technol.* **2006**, *201*, 2217. (c) Luan, H.; Alshareef, H. N.; Harris, H. R.; Wen, H. C.; Choi, K.; Senzaki, Y.; Majhi, P.; Lee, B.-H. *Appl. Phys. Lett.* **2006**, *88*, 142113. (d) Varesi, E.; Pavia, G.; Zenkevich, A.; Lebedinskii, Y.; Besana, P.; Giussani, A.; Modelli, A. *J. Phys. Chem. Solids* **2007**, *68*, 1046.

(18) (a) Vepřek, S.; Reiprich, S. *Thin Solid Films* **1995**, *268*, 64. (b) Blanquet, E.; Dutron, A. M.; Ghetta, V.; Bernard, C.; Madar, R. *Microelectron. Eng.* **1997**, *37/38*, 189.

(19) Park, H.-L.; Byun, K.-M.; Lee, W.-J. *Jpn. J. Appl. Phys.* **2002**, *41*, 6153.

(20) (a) Min, J. S.; Park, J. S.; Park, H. S.; Kang, S. W. *J. Electrochem. Soc.* **2000**, *147*, 3868. (b) Park, J. S.; Kang, S. W. *Electrochem. Solid-State Lett.* **2004**, *7*, C87. (c) Park, J. S.; Kang, S. W.; Kim, H. J. *J. Vac. Sci. Technol., B: Microelectron. Nanometer Struct.* **2006**, *24*, 1327.

(21) (a) Kim, M.-K.; Han, Y.-S.; Kim, M.-S.; Yang, S.-H.; Lei, X. *Air Products and Chemicals*, U.S. Pat. Appl. Publ. (2008), US 20080318443, A1 20081225. (b) Lei, X.; Thridandam, H.; Cuthill, K. S.; Hochberg, A. K. *Air Products and Chemicals*, Eur. Pat. Appl. (2006), EP 1691400, A1 20060816. (c) Lei, X.; Thridandam, H.; Xiao, M.; Bowen, H. R.; Gaffney, T. R. *Air Products and Chemicals*, U.S. Pat. Appl. Publ. (2008), US 20080145535, A1 20080619.

(22) (a) Lei, X.; Xiao, M.; Thridandam, H.; Cuthill, K. S. *Air Products and Chemicals*, U.S. Pat. Appl. (2006), US 7064224, B1 20060620. (b) Norman, J.A. T.; Lei, X. *Air Products and Chemicals*, Eur. Pat.Appl. (2007), EP 1772460, A1 20070411.

(23) McElwee-White, L. *Dalton Trans.* **2006**, 5327.

(24) (a) Park, J. W.; Lee, C. H.; La, Y. H.; Park, S. J. *Organometallics* **1998**, *17*, 3648. (b) Daniele, S.; Hitchcock, P. B.; Lappert, M. F. *Chem. Commun.* **1999**, 1909. (c) Xue, Z. L.; Yu, X. H. *Inorg. Chem.* **2005**, *44*, 1505. (d) Heyduk, A. F.; Blackmore, K. J.; Ketterer, N. A.; Ziller, J. W. *Inorg. Chem.* **2005**, *44*, 468. (e) Xue, Z. L.; Yu, X. G.; Chen, S. J.; Wang, X. P.; Chen, X. T. *Organometallics* **2009**, *28*, 4269. (f) Jordan, R. F.; Lococo, M. D.; Lee, H. *J. Mol. Struct.* **2009**, *920*, 363. (g) Hoffman, D. M.; Jimenez, E. D.; Javed, S. *Inorg. Chim. Acta* **2009**, *362*, 385. (h) Male, N. A. H.; Thornton-Pett, M.; Bochmann, M. *J. Chem. Soc., Dalton Trans.* **1997**, 2487. (i) Liu, D. S.; Li, J. F.; Weng, L. H.; Huang, S. P.; Tong, H. B. *Acta Crystallogr., Sect. E* **2002**, *58*, M510. (j) Kim, K.; Jeon, Y. M.; Heo, J.; Lee, W. M.; Chang, T. H. *Organometallics* **1999**, *18*, 4107. (k) Gibson, V. C.; Kimberley, B. S.; White, A. J. P.; Williams, D. J.; Howard, P. *Chem. Commun.* **1998**, 313.

(25) Choquette, D. M.; Timm, M. J.; Hobbs, J. L.; Rahim, M. M.; Ahmed, K. J.; Planalp, R. P. *Organometallics* **1992**, *11*, 529.

(26) Bowser, J. R.; Neilson, R. H.; Wells, R. L. *Inorg. Chem.* **1978**, *17*, 1882.

(27) Bradley, J. S.; Cheng, F.; Archibald, S. J.; Supplit, R.; Rovai, R.; Lehmann, C. W.; Krüger, C.; Lefebvre, F. *Dalton Trans.* **2003**, 1846.

(28) Farrugia, L. J. *J. Appl. Crystallogr.* **1999**, *32*, 837.

(29) Edwards, D. A.; Harker, R. M.; Mahon, M. F.; Molloy, K. C. *J. Mater. Chem.* **1999**, *9*, 1771.

(30) Lorber, C.; Choukroun, R.; Vendier, L. *Eur. J. Inorg. Chem.* **2006**, 4503.

(31) Thorn, D. L.; Nugent, W. A.; Harlow, R. L. *J. Am. Chem. Soc.* **1981**, *103*, 357.

(32) Collier, P. E.; Blake, A. J.; Mountford, P. *J. Chem. Soc., Dalton Trans.* **1997**, 2911.

(33) Gao, M.; Tang, Y.; Xie, M.; Qian, C.; Xie, Z. *Organometallics* **2006**, *25*, 2578.

(34) Hughes, A. K.; Meetsma, A.; Teuben, J. H. *Organometallics* **1993**, *12*, 1936.

(35) Wagner, O.; Jansen, M.; Baldus, H. P. *Z. Anorg. Allg. Chem.* **1994**, *620*, 366.

(36) (a) Ren, G. M.; Shang, D. L.; Guo, J. P. *Acta Crystallogr., Sect. E* **2007**, *63*, m793. (b) Atagi, L. M.; Hoffman, D. M.; Smith, D. C. *Inorg. Chem.* **1993**, *32*, 5084. (c) Walther, D.; Schramm, F.; Theyssen, N.; Beckert, R.; Gorls, H. *Z. Anorg. Allg. Chem.* **2002**, *628*, 1938.

(37) Chen, J. *Acta Crystallogr., Sect. E* **2008**, *64*, M938.
(38) Schumann, H.; Gottfriedsen, J.; Dechert, S.; Girgsdies, F. *Z. Anorg. Allg. Chem.* **2000**, *626*, 747.
(39) Chen, J.; Cao, K. N.; Guo, J. *Acta Crystallogr., Sect. E* **2007**, *63*, M3107.
(40) Chen, J. *Acta Crystallogr., Sect. E* **2009**, *65*, M1307.
(41) Fix, R. M.; Gordon, R. G.; Hoffman, D. M. *Chem. Mater.* **1990**, *2*, 235.
(42) García-González, L.; Hernández-Torres, J.; Mendoza-Barrera, C.; Meléndez-Lira, M.; García-Ramírez, P. J.; Martínez-Castillo, J.; Sauceda, A.; Herrera-May, A. L.; Saldaña, J. M.; Espinoza-Beltrán, F. J. *J. Mater. Eng. Perform.* **2008**, *17*, 580.
(43) Kamiyama, S.; Kurosawa, E.; Nara, Y. *J. Electrochem. Soc.* **2008**, *155*, H373.
(44) Ramqvist, L.; Hamrin, K.; Johansson, G.; Fahlman, A.; Nordling, C. *J. Phys. Chem. Solids* **1969**, *30*, 1835.
(45) Yang, G.-R.; Zhao, Y.-P.; Hu, Y. Z.; Chow, T. P.; Gutmann, R. J. *Thin Solid Films* **1998**, *333*, 219.
(46) Zhang, L. S.; Terauchi, S.-Y.; Azuma, Y.; Fujimoto, T. *Surf. Interface Anal.* **2008**, *40*, 1701.
(47) Milošev, I.; Strehblow, H.-H.; Navinšek, B. *Surf. Interface Anal.* **1998**, *26*, 242.
(48) (a) Lu, F.-H.; Chen, H.-Y. *Thin Solid Films* **1999**, *355*−*356*, 374. (b) Jiang, N.; Zhang, H. J.; Bao, S. N.; Shen, Y. G.; Zhou, Z. F. *Physica B* **2004**, *352*, 118.
(49) Prieto, P.; Galán, L.; Sanz, J. M. *Phys. Rev. B* **1993**, *47*, 1613.
(50) Kato, H.; Nango, T.; Miyagawa, T.; Katagiri, T.; Seol, K. S.; Ohki, Y. *J. Appl. Phys.* **2002**, *92*, 1106.
(51) Renault, O.; Samour, D.; Damlencourt, J.-F.; Blin, D.; Martin, F.; Marthon, S.; Barrett, N. T.; Bresson, P. *Appl. Phys. Lett.* **2002**, *81*, 3627.
(52) Watanabe, Y.; Yoshida, S.; Kita, Y.; Shimura, T.; Watanabe, H.; Yasutake, K.; Akasaka, Y.; Nara, Y.; Yamada, K. *Sci. Technol. Adv. Mater.* **2007**, *8*, 219.